
# INSTITUTE FOR AEROSPACE STUDIES

## UNIVERSITY OF TORONTO



# EVALUATION OF THE EFFECTS OF ATOMIC OXYGEN ON POLYMERIC MATERIALS

by

R. C. Tennyson, J. B. French, L. Kok and J. Kleiman

University of Toronto
Institute for Aerospace Studies

Final Report
Under Contract No. OST83-00245

Submitted to the Communications Research Centre
Shirley Bay
Ottawa

April 1984

Government of Canada | Gouvernement du Canada

Department of Communications

DOC CONTRACTOR REPORT DOC-CR-84-039

DEPARTMENT OF COMMUNICATIONS - OTTAWA - CANADA

SPACE PROGRAM

TITLE: Evaluation of the Effects of Atomic Oxygen on Polymeric Materials

AUTHOR(S): R.C. Tennyson, J.B. French, L. Kok, and J. Kleiman

ISSUED BY CONTRACTOR AS REPORT NO:

PREPARED BY: University of Toronto Institute of Aerospace Studies (UTIAS)

DEPARTMENT OF SUPPLY AND SERVICES CONTRACT NO: OST83-00245

DOC SCIENTIFIC AUTHORITY: Dr. D.G. Zimcik
Space Mechanics Directorate

CLASSIFICATION: Unclassified



DATE: April 1984

(1)

# EVALUATION OF THE EFFECTS OF ATOMIC OXYGEN ON POLYMERIC MATERIALS

by

R. C. Tennyson, J. B. French, L. Kok and J. Kleiman

University of Toronto
Institute for Aerospace Studies

Final Report
Under Contract No. OST83-00245

Submitted to the Communications Research Centre
Shirley Bay
Ottawa

April 1984

ACKNOWLEDGEMENT

The authors wish to acknowledge the financial support for this study received from the Communications Research Centre, Shirley Bay, Ottawa, under Contract No. OST83-00245. Furthermore, we are most appreciative to Dr. N. Salansky and Dr. R. Park (3M Canada, Inc.) who provided access to the scanning electron microscope facility located at the Institute for Aerospace Studies. In addition, Dr. A. Neumann and Mr. R. Smith of the Department of Mechanical Engineering at the University of Toronto provided the facilities for measuring the surface tension characteristics of the samples. Finally, the setup of the atomic oxygen beam apparatus was made possible by the extensive technical assistance rendered by Mr. J. Leffers and Dr. S. Merza.

ABSTRACT

A nozzle beam facility utilizing microwave discharge on a helium carrier gas seeded with oxygen to produce atomic oxygen fluxes of the order of $10^{15}$ atoms/$cm^2$-sec is described in this report. In addition, limited test results obtained from exposing a graphite/epoxy composite and Kapton (H) film are presented in terms of mass loss measurements and changes in surface morphology.

SYMBOLS

| | |
|---|---|
| $a$ | local speed of sound |
| $A$ | area |
| $C_p$ | specific heat at constant pressure |
| $C_v$ | specific heat at constant volume |
| $I$ | molecular flux per solid angle (molecules/steradian/sec) |
| $K$ | degrees Kelvin |
| $Kn$ | Knudsen number |
| $m$ | mass |
| $M_f$ | freezing Mach number |
| $n$ | number density |
| $N_{AV}$ | Avogadro's number, $6.02 \times 10^{23}$/mole |
| $P$ | pressure |
| $R$ | universal gas constant, $8.314 \times 10^3$ J/kilomole/K |
| $T$ | temperature |
| $u$ | molecular weight of gas |
| $V$ | velocity |
| $x$ | distance from the orifice |
| $\alpha$ | dissociation fraction |
| $\gamma_{LV}$ | surface tension at liquid-vapour interface |
| $\gamma_{SL}$ | surface tension at solid-liquid interface |
| $\gamma_{SV}$ | surface tension at solid-vapour interface |
| $\sigma_{EX}$ | total flux from orifice (molecules/sec) |
| $\sigma_t$ | flux per unit area (atoms/cm$^2$-sec) |
| $\Omega_t$ | solid angle from nozzle to target |
| $\lambda$ | mean free path |
| $\gamma$ | ratio of specific heats, $C_p/C_v$ |
| $\theta$ | polar angle with orifice exit as centre |

## INTRODUCTION

An orbiting satellite can be regarded as a body in free molecular flow. One generally characterizes this domain in terms of the Knudsen number (Kn) (i.e., the ratio of the mean free path of a gas/characteristic dimension of the body) which, for the upper atmosphere, is very large. The lower boundary of the free molecular flow region is usually taken at Kn > 10, which is true for all altitudes greater than 125 km (ref. 1). In this regime, the probability of gas-gas collisions is small. One can refer to fig. 1 to see the dominant atmospheric constituent concentrations as a function of altitude. For example, it is of interest to note that at 200 km, the orbital velocity is $7.78 \times 10^5$ cm/sec and the mean free path for nitrogen corresponds to $7 \times 10^4$ cm. Taking the atmospheric density to be about $2 \times 10^9/cm^3$ at 200 km, the mean free path is about 700m. Thus Kn = 700 for a body of 1m dimension (ref. 1). For satellite-gas collision studies, this orbital velocity corresponds to impact gas energies of 0.34, 4.40 and 5.03 electron volts (eV) for hydrogen, nitrogen and oxygen atoms, respectively (ref. 1).

Many satellites orbit at altitudes ranging from 125 km - 600 km where atomic oxygen is the most active and dominant species interacting with the surface of the vehicle. With the advent of the Space Transportation System flights (i.e., Space Shuttle), one has now been presented with the opportunity to witness the effects of gas-surface interactions on a variety of spacecraft materials. For example, materials housed in the shuttle's payload bay have been exposed to an atomic oxygen flux estimated to be in the range of $10^{14}$ to $10^{15}$ atoms/$cm^2$/sec. These materials include Teflon-coated Beta fabric and Kapton (primary constituents of thermal insulation blankets), various thermal and identification paints, and various graphite/epoxy structural members (refs. 2, 3). Some physical observations to-date include: Kapton exhibited a colour

change from its inherent gold to a milky yellow; the paints showed what appeared to be rapid aging, as they were easily removed by lightly wiping the surface. Mass loss for the Kapton was determine to be 4.3 to 4.7 percent and was evident on over 35 percent of all the thermal insulation blankets (refs. 2, 3). Areas behind supporting members or brackets (with respect to the velocity vector) were protected from the effects, as evidenced by strong shadow patterns on the painted surfaces. The backside of the exposed surfaces showed little change. For further details and information on the effects of atomic oxygen on a variety of materials flown on STS missions (3 to 8), one can refer to Table 1 (taken from ref. 3).

Based on STS test data and the observations noted above, a need clearly exists to simulate the environmental conditions to study this phenomenon. From a design viewpoint, it is essential to qualify materials for spacecraft applications subject not only to atomic oxygen bombardment, but other radiation effects and synergisms that may occur as well.

## NOZZLE BEAM GENERATION SYSTEMS

### INTRODUCTION

There are two main types of molecular beams used for continuous high density particle flow simulation; the classical effusive beam and the nozzle beam systems (refs. 4, 5). The effusive beam is simply formed by particles effusing through a slit or orifice from a low pressure stagnation source into a vacuum system (fig. 2). The mean velocity in such a beam is a strong function of the throat temperature and can thus be calculated from the source equilibrium Maxwellian distribution (ref. 6). The nozzle beam, on the other hand, has molecules emanating from a stagnation source, which undergo a free jet expansion at the nozzle exit into the vacuum chamber, where the flow is

essentially in the free molecular flow regime. The beam is accelerated as it expands and the molecules' vibrational, translational and rotational motions are converted to translational energy along the axis of the nozzle (ref. 4). The higher the pressure, the more complete is the conversion to translational energy.

One advantage of a nozzle beam is that the velocity distribution is smaller (when compared to the bulk beam velocity) than that for an effusive beam. Higher fluxes can also be realized as well as a higher terminal velocity in the final beam. The method of 'seeding' the beam can further increase the velocity of the molecular beam. This involves using a lighter gas, such as He, as a carrier gas with a small percentage of the heavier gas of interest, $O_2$ in this case. The lighter gas' higher terminal velocity for a given source temperature, $T_o$, is given by

$$(1/2)\ mV^2 = (3/2)\ T_o R/N_{av} \qquad (1)$$

The fast moving carrier gas will, however, accelerate the heavier gas by collisions, and if no slip occurs, speeds close to the terminal velocity of the lighter gas can be realized.

The latter beam system with the seeding technique was employed using a facility configuration developed by Lam (ref. 7). A heated beam can also increase the velocity but no ohmic heating was incorporated in this design due to its additional complexities, as experienced by Lam with thoria cavities (ref. 4).

EXPERIMENTAL APPARATUS

The experimental apparatus utilized by Lam (ref. 7) involving the generation of a high-velocity mono-energetic nozzle beam containing atomic oxygen was employed as shown in figs. 3-8. Microwave power discharge on a helium carrier gas seeded with 8% oxygen flowing through a quartz tube provided

a partially dissociated oxygen flux into a vacuum chamber containing a sample target. There are two major advantages associated with the microwave method of producing atomic oxygen. Firstly, since no intermittent electrode discharges are present, one obtains a "clean", uncontaminated beam containing a constant supply of atomic oxygen (ref. 7). Secondly, after ionization of the gas by the microwave discharge, dissociation occurs at relatively low temperatures (850 ~ 1000 K) and thus the nozzle can be made from quartz. This provides a clean and stable surface which is very inefficient for recombining gas radicals (ref. 7). One should note that this method of dissociation by glow-discharge does introduce excited species which are retained in the beam, as contrasted with the thermal dissociation process which maintains all of the gas atoms in the ground state electronically (ref. 4). However, to create atomic oxygen by thermal dissociation requires very high temperatures (up to 3000 K) to overcome the 5.12 eV chemical bond of molecular oxygen (see Lam, ref. 4). On the other hand, higher dissociation values (~55%) and beam velocities (~3.8 km/sec) can be achieved using this approach (ref. 4), compared to the microwave discharge method.

The facility employed in this investigation utilized a Microtron 200 microwave power geneator unit (fig. 4) operating at a frequency of 2450 MHz (12.5 cm) with a rated power from 20 to 200 watts. A Tesla coil was used to initiate the microwave-induced plasma in the tunable cavity. The cavity was tuned so that the reflected power to the microwave generating unit was minimized. This state corresponds to the maximum efficiency of the process and is characterized by the glow discharge in the tuning cavity (fig. 5). It should be emphasized, however, that the continuous wave magnetron can only withstand 75 watts reflected power for a short period or 40 watts continuously. Since long term exposure tests were required (i.e., operating periods of

several weeks continuous running), the maximum power setting was maintained at 30 watts. Thus if the microwave plasma was accidentally extinguished, the maximum reflected power would not exceed the 40 watts limit.

The test chamber consisted of a Quick-fit Visible Flow vacuum vessel (fig. 6) fitted with a Balzers pumping system. The pumping occurred in two stages; the first handled by a roughing pump, the second by a diffusion pump. The former obtained pressures to 40 millitorr whereas the latter two-stage, water cooled trap diffusion pump could attain a pressure of $4.0 \times 10^{-5}$ torr with the beam in operation. Pressure readings were obtained through a Granville-Phillips ionization gauge fitted to the upper arm of the vacuum vessel.

Opposite to the entry port of the gas beam, an Aero Vac Vacuum Analyzer (fig. 7) was fitted, enabling the scanning of the mass spectrum to identify residual gases. Since the ionizer of this mass spectrometer faced directly into the beam flux, it would ionize only the background gases if the beam was blocked or "flagged", or a combination of the beam and background gases in the "unflagged" configuration. The ionization spectrometer can be calibrated for various pressure ranges from $10^{-4}$ to $10^{-10}$ torr. Scanning over the mass spectrum range (70-12 amu) can be done automatically or manually. The latter allows the spectrometer to be set to monitor one element during various phases of the nozzle beam operation.

The flow of gas was controlled by a series of regulator valves (fig. 8) with a constant mass flow rate being set by a Nupro needle valve. At this point the pressure was measured using a Wallace & Tiernan absolute pressure gauge.

## ESTIMATION OF ATOMIC OXYGEN FLUX

It is difficult to measure the degree of oxygen dissociation achieved in the cavity itself (unless optical spectroscopy is available and carefully calibrated). Since the primary requirement for these tests is to know the actual beam fluxes of atomic and molecular oxygen, it was appropriate to start by using the available residual gas analyser, mounted on the opposite chamber wall so that its open ion source could be exposed to the atomic beam.

It should be emphasized that it is by now well-documented that microwave discharges operating under the conditions used in these tests typically produce dissociation fractions of the order of 1% ~ 5%. The addition of about 1% $H_2O$ to the input gas can, however, increase the dissociation up to 20% (ref. 7). Based on Lam's experiments using a similar facility (ref. 7), it is estimated that the dissociation fraction is approximately 3%.

Although the beam facility is not capable of achieving the orbital energy level for atomic oxygen, it can provide the desired flux. Based on the free jet parameters and sample location, one can estimate the beam flux, as outlined in the Appendix.

Calculations show that the oxygen flux increases exponentially with increasing percentage of $O_2$ in the mixture (fig. 9). This would indicate that the optimum would be to use an all-oxygen gas mixture, although the beam velocity would decrease as described earlier. On the other hand, the lower the percentage of $O_2$ in the mixture, the higher the degree of dissociation and hence the lower the residual undissociated species content. In terms of sample placement, it can be seen (fig. 10) that the atomic oxygen flux falls off with distance squared. From these considerations, a low percentage mixture and location of the sample at the nozzle orifice would seem optimal. This,

however, is not necessarily the case due to the formation of a bow shock wave which can reduce the flux impinging on the sample.

The initial experiments described in this report were conducted with the sample located 3 cm from the orifice. It should be noted that the flux is not onstant over the sample area, but varies according to (ref. 8);

$$n(x,\theta) = 0.643\ n_0[\cos^2(1.1510]\cdot(x/R_0)^{-2} \qquad (2)$$

where $\theta$ is the polar angle coordinate with the orifice exit as centre. The corresponding variaion in flux density is shown in fig. 11.

Calculations performed in the Appendix estimate the incident atomic oxygen flux at $\sim 10^{15}$ atoms/cm$^2$-sec at the beam centre. Other characteristics of the beam are: Mach No: 1.9, and Energy: 0.14 eV. It should be noted that the flux level probably represents an over-estimate due to the presence of a bow shock. Future experiments will involve locating the sample about 30 cm from the orifice. Although the flux will decrease according to fig. 10, it is intended to determine if indeed the presence of the shock wave had a significant effect on reducing the incident beam flux on the target.

## EFFECTS OF ATOMIC OXYGEN ON SAMPLES

### SAMPLE EXPOSURE

Two types of samples were exposed to the atomic oxygen beam: Kapton, a polypyromelitimide manufactured by DuPont, and Hercules ASI/3501-6 graphite/epoxy composite. The Kapton was used mainly as a calibration sample; since data on the effects of atomic oxygen had already been documented by Leger (refs. 2, 3). Throughout the duration of the exposure, mass spectrographs were taken to determine the constituents being released from the sample by the oxidation and/or impact process. Immediately after exposure, the mass loss was determined for each of the samples. The surface activation energy was then

measured to provide an indication of surface changes. Scanning electron microscope images were also obtained to determine changes in surface morphology.

MASS SPECTROGRAPHS

After the initial pump-down of the vacuum vessel, a mass spectrograph was taken as a control (fig. 12). The elements shown largely result from residual amounts of gas from the atmosphere, although the hydrocarbon peaks are associated with the silicone oil used in the roughing pump. Once this pump is turned off, upon activation of the diffusion pump the presence of these hydrocarbons became imperceptible as testing proceeded.

Graphite Sample

The sample, once installed, was subjected to the atomic oxygen beam. Of concern was whether there was a detectable difference between having the atomic oxygen interacting with the sample as compared to having the carrier gas impinging on the surface. A mass spectrograph (fig. 13) was taken with the microwave generator on and off during the initial exposure tests on a graphite/epoxy sample. The purpose was to separate out the effects of the carrier gas mixture and that of atomic oxygen. As can be seen in fig. 13, increases in the levels of the hydrocarbons occurred when atomic oxygen was present, accompanied by the appearance of ethane ($C_2H_6$) and the $C_2H_5$ radical. In addition, increases in the $H_2O$ and OH peaks probably resulted from the combination of O and $O_2$ with radical H atoms released in the reaction of atomic oxygen with the sample. As testing progressed, the levels of these latter peaks decreased, as can be seen in fig. 14. This spectrograph, taken just prior to sample removal after 265 hours of exposure, exhibits a marked increase in the methane peak ($CH_4$). Thus it would appear that there is an increased rate of reaction with time of atomic oxygen with the graphite/epoxy material.

Furthermore, a mass spectrograph (fig. 15) taken at the same time only with the atomic oxygen source off, indicates the presence of the same $CH_4$ peak, but the $CO_2$, $CH_3$, $C_2H_6$ and C peaks have disappeared. The lingering methane peak probably demonstrates a continued reaction producing this outgassing product, even though the oxygen source has been terminated. With time, the methane peak was observed to subside.

Kapton Sample

A similar set of spectrographs was taken while the Kapton was being exposed (figs. 16 and 17). Hydrocarbon reaction products were also released when Kapton was bombarded with atomic oxygen but their number was less numerous. Only carbon, ethane, carbon monoxide and methane were released. The peak of the methane was much larger initially than that for the graphite/epoxy, although it also remained as an outgassing product once the atomic oxygen beam was extinguished (fig. 17).

MASS LOSS MEASUREMENTS

Table 2 summarizes the samples tested, their dimensions, exposure times and masses. Both the control samples and targets were weighed using a microbalance (sensitive to $\pm 1 \times 10^{-6}$ gm) before and after exposure. The major difficulty in assessing mass loss due to atomic oxygen impingement is the uncertainty associated with the target beam area and the net surface area subject to outgassing. As a result, two models were used to estimate probable mass losses:

(a) the target is assumed to outgas over its full surface area;

(b) the target is assumed to outgass over its full surface area less 1 $cm^2$ associated with the atomic oxygen beam.

A summary of these calculated % mass losses and mass loss rates due to vacuum alone and atomic oxygen is contained in Table 3. Note that the control

samples provide the vacuum baseline data. From Table 3 it is evident that neither model predicts a mass loss for Kapton, even though a change in surface morphology has occurred (as described later). On the other hand, if one assumes for example that the target area facing the beam does not outgass, then indeed one arrives at a % mass loss of 0.023 and a mass loss rate/unit area of $\sim 1.12 \times 10^{-10}$ gms/cm$^2$-sec. Clearly more effort must be directed towards ascertaining the correct outgassing model for targets subject to molecular beam impingement.

SURFACE ACTIVATION ENERGIES

After removal, the samples were kept in a moisture-free container to prevent re-absorption of water vapour from the atmosphere which could possibly change the surface characteristics of the sample. The surface activation energy can be inferred by measuring the contact angle between a drop of fluid and the surface of a sample. The fluid used to determine the contact angle was distilled water, which tends to give the best results over a wide range of differing materials (ref. 9).

The procedure involved placing a drop of liquid on the sample and determining the angle between the surface of the sample and a line tangent to the drop at the bubble-surface interface. The equipment for the 'drop test' is composed of a horizontal platform on which the sample is mounted. A micro-pippette is used to dispense the drop onto the surface, after which a telescope with a protractor eyepiece can be used to determine the contact angle. An illumination source is provided so that the droplet-surface interface can be easily discerned. Parallax can be eliminated if the telescope is mounted on a track that allows two degrees of freedom (ref. 10). A summary of the contact angles measured is found in Table 4.

From Young's equation:

$$\gamma_{SV} - \gamma_{SL} = \gamma_{LV} \cos\theta \qquad (3)$$

$$\gamma_{SL} = \frac{[[(\gamma_{SV})^2 + (\gamma_{SL})]^2]^{1/2}}{1 - 0.015(\gamma_{SV} \times \gamma_{LV})^{1/2}} \qquad (4)$$

Taking $\gamma_{LV}$ = 72.5 mJ/m$^2$ for room temperature conditions, the surface tension of the interface ($\gamma_{SL}$) can then be calculated (Table 3). Since there is a marked change in surface tension, a change in surface energy is inferred, and hence a change in the characteristic morphology of the sample due to atomic oxygen exposure has occurred.

SCANNING ELECTRON MICROSCOPE STUDY

To detect surface morphology changes, an SEM was employed. The graphite/epoxy was analyzed directly due to its conductivity. However, the Kapton, being essentially an insulator, required a gold film to be deposited on its surface before being scanned. The SEM provided flat images as well as modulated ones that produced a 'contour map' of the area being observed. It was this latter feature that was very useful in studying the Kapton surface.

Graphite/Epoxy Sample

An unexposed, unprepared section of graphite/epoxy composite material (fig. 18) clearly shows the carbon fibres, approximately 10 microns in diameter, covered with epoxy. The target sample was polished so that a 'planar' surface could be obtained, thus providing better depth-of-field resolution for the SEM (fig. 19). After approximately 265 hours of exposure to

atomic oxygen, the sample was removed and images were taken of the exposed region (fig. 20). It is evident in comparing the exposed and unexposed regions that the atomic oxygen reacted primarily with the epoxy and essentially removed the top layer down to the graphite fibres. Fibre breakage in the exposed areas was also observed to be more pronounced than in unexposed areas.

Kapton (H) Sample

The SEM images of Kapton revealed a much different morphology than the graphite/epoxy material. For example, consider first the control sample (figs. 21, 22) as viewed in the normal and Y-modulated SEM modes. In the direct 'picture mode' of operation (fig. 21), one sees a few lines and isolated dark and 'light' spots. However, in the modulated mode images (fig. 22), the lines correspond to ridges (probably associated with surface scratches on the Kapton film), with the dark and light spots depicting depressions and hills, respectively. Two other modulated views showing similar surface features on the control sample are shown in figs. 23 and 24.

When one examines the target sample after exposure to approximately 187 hours of atomic oxygen, one finds regions of intense dark spots (figs. 25, 27) which, when viewed in the modulated mode, clearly depict large depressions (figs. 26, 28). These areas are quite different from the depressions observed on the control sample and exhibit 'pitting' characteristics. It would appear that the atomic oxygen has reacted with the Kapton to produce this change in surface morphology.

## CONCLUDING REMARKS

An atomic oxygen nozzle beam facility has been assembled capable of providing a beam flux of about $10^{15}$ atoms/cm$^2$-sec at an energy level of ~0.14 eV. Although the system is providing dissociation fractions around 1% ~ 5%,

the upper limit can be significantly increased (up to 20%) by the addition of ~1% $H_2O$ to the input gas. Furthermore, higher energy levels can probably be attained by reducing the vacuum state below the current operating level of ~$10^{-5}$ torr.

Test results to date clearly show a change in surface morphology for graphite/epoxy and Kapton materials exposed to a total atomic oxygen fluence of ~$10^{21}$ atoms/$cm^2$ and $7\times10^{20}$ atoms/$cm^2$, respectively. Note however that these fluence levels are probably too high, since the influence of the bow shock has not been considered in terms of reducing the incident beam flux on the target. Mass loss measurements based on these limited results were obtained only for graphite/epoxy (approximately 0.13% with a mass loss rate/unit area of ~$6\times10^{-10}$ gms/$cm^2$-sec). Insufficient exposure time for the Kapton film produced no significant mass loss and thus repeat testing is necessary.

REFERENCES


1. Jackson, D. P.: A Theory of Gas-Surface Interactions at Setellite Velocities. UTIAS Tech. Note No. 134, Nov. 1968.

2. Leger, L. J.: Oxygen Atom Reaction with Shuttle Materials at Orbital Altitudes. NASA TM 58246, L.B.J. Space Center, Houston, Texas, 1982.

3. Leger, L. J.; Visentine, J. T.; and Kuminecz, J. F.: Low Earth Orbit Atomic Oxygen Effects on Surfaces. proc. AIAA 22nd Aerospace Sciences Meeting, Paper No. 84-0548, Reno, Nevada, U.S.A., Jan. 1984.

4. Lam, Kalvin.: A Hypersonic Atomic Oxygen Molecular Beam Source. Doctoral Thesis, Institute for Aerospace Studies, University of Toronto, Canada, 1976.

5. French, J. B.: Molecular Beams for Rarefied Gasdynamic Research. AGARDograph 112, NATO, 1966.

6. Sears, F.; and Salinger, G.: Thermodynamics, Kinetic Theory and Statistical Thermodynamics (3rd Edition). Addison-Wesley Publishing Co., Don Mills, Canada, 1975.

7. Lam, Kalvin.: Development of a Nozzle Beam Containing Atomic Oxygen. UTIAS Technical Note No. 153, University of Toronto, Canada, 1970.

8. Ashkenas, H.; and Sherman, F. S.: In Rarefied Gas Dynamics, Ed. J. H. de Leeuw, VII, Academic Press, New York, 1966.

9. Neumann, A. W.; and Good, R. J.: Techniques of Measuring Contact Angles. Surface and Colloid Science (Vol. 11): Experimental Methods. Plenum Press, New York, 1979.

10. Hansen, R. H.; Pascale, J. V.; et al: Effect of Atomic Oxygen on Polymers. Journal of Polymer Science, Vol. 3, 1965, pp. 2205-2214.

## APPENDIX: MODEL CALCULATIONS OF FREE-JET EXPANSION CHARACTERISTICS

Model calculations concerning the free-jet expansion of the nozzle beam in the test chamber are presented below:

(1) Total flux of molecules, $\sigma_{ex}$, issued out of source tube orifice per unit time.

$$\sigma_{ex} = [2/(\gamma+1)^{(\gamma+1)/2(\gamma-1)} n_o a_o A_o$$

where

$$a_o = (\gamma R T_o/u)^{1/2}$$

The apparent ratio of the specific heats, $\gamma$, is:

$$\gamma = (0.92 \times C_{p_{He}} + 0.08 \times C_{p_{O_2}})/(0.92 \times C_{v_{He}} + 0.08 \times C_{v_{O_2}})$$

for a 92% He and 8% $O_2$ mixture.

Given that,

$$C_{p_{He}} = 2.50\ R, \quad C_{v_{He}} = 1.51\ R, \quad C_{p_{O_2}} = 3.53\ R, \quad C_{v_{O_2}} = 2.52\ R$$

then $\gamma = 1.627$ and

$$R_s = R/u$$
$$= 8.3143 \times 10^3 \text{ Nm kilomole}^{-1}\text{K}^{-1}/(4 \times 0.92 + 32 \times 0.08)\text{kg/kmole}$$
$$= 1.3324 \times 10^3 \text{J}$$

with $T_o$ = 293 K, $a_o = (1.627 \times 1.3324 \times 10^3 \times 293)^{1/2}$ = 796.97 m/sec,

$n_o = N(273/T_o)(P_o/760)$

which for $P_o$ = 1.9 torr, $n_o = 2.35 \times 10^{16}$ molecules/cc

For an orifice diameter, $D_o$, of .06096 cm (24/1000"), $A_o = 2.9186 \times 10^{-3} cm^2$.

Therefore, $\sigma_{ex} = 8.766 \times 10^{18}$ molecules/sec.

(2) Total molecular flux impinging on the sample per unit time per unit area.

$$I_{ex} = 0.6276\ \sigma_{ex} \text{ molecules/steradian/sec}$$

$$= 5.50 \times 10^{18} \text{ molecules/steradian/sec}$$

The solid angle, $\Omega_t$, from the nozzle subtended by a 1 $cm^2$ target area 3 cm from the orifice is given by: $\Omega_t = 1/3^2 = .111$ steradians

Thus, $\sigma_t = .111\ I_{ex} = 6.11 \times 10^{17}$ molecules/$cm^2$/sec. Now, only 8% of these molecules are $O_2$ of which approximately 3% splits into 2-O atoms. Hence

$$\sigma_{t_O} = \sigma_{t_{O_2}} \times \alpha \times 2 = 6.11 \times 10^{17} \times 0.08 \times 0.03 \times 2$$

$$= 2.93 \times 10^{15} \text{ atoms/cm}^2\text{/sec}$$

(3) The energy of the impinging atomic oxygen atoms can be calculated if a no-slip condition is assumed between the He and oxygen atoms. That is to say, all particles take on the sonic velocity of the He gas.

The freezing Mach number is given by: $M_f = 1.18\ K_{no}^{-(\gamma-1)/\gamma}$

but $K_{no} = \lambda_o/D_o$, $\lambda_o = 1/(n_o \times d^2 \times \pi \times 2^{1/2})$

where d is the average molecular diameter:

$$d = 2(1.1\times10^{-8}\times0.92 + 1.9\times10^{-8}\times0.08)$$
$$= 2.328\times10^{-8}\text{cm}$$

Thus $\lambda_o = 1/56.58$ cm; $K_{no} = 0.2899$, giving $M_f = 1.898$.

$$v = M_f a_o[1 + (\gamma-1)/2M_f^2]^{-1/2}$$
$$= 1.203\times10^3 \text{ m/sec}$$
$$a_{o_{He}} = (\gamma RT_o/u)^{1/2} = 1008.17 \text{ m/sec}$$

Hence, $V_{He} = 1.3135\times10^5$ cm/sec. Since $E = \frac{1}{2}\ mV^2$ then

$$E_0 = \frac{1}{2}[15.994\times1.66\times10^{-27}\times(1.3135\times10^3)^2]$$
$$= 2.29\times10^{-20} \text{ J}$$
$$= 0.143 \text{ eV}$$

TABLE 1. SUMMARY OF ATOMIC OXYGEN REACTION EFFECTS
FOR VARIOUS THIN FILMS USED ON SPACECRAFT
(From Ref. 3)

| Shuttle Flight | Thin Film Material | Thickness μm (a) | Thickness Loss μm | Fluence $10^{20}$ atoms/cm$^2$ | Reaction Efficiency $10^{-24}$ cm$^3$/atom (b) |
|---|---|---|---|---|---|
| STS-3 | Kapton TV Blanket | 12.7 | 4.4 | 2.16 | 2.0 |
| | Kapton, OSS-1 Blanket | 25.4 | 5.5 | 2.16 | 2.5 |
| STS-4 | Kapton | 7.6 | 1.8 | 0.65 | 2.8 |
| Witness | Kapton | 12.7 | 1.6 | 0.65 | 2.7 |
| Samples | Kapton | 25.4 | 1.7 | 0.65 | 2.6 |
| | Mylar | 12.7 | 1.8 | 0.65 | 2.8 |
| | Teflon FEP & TFE | 12.7 | 0.07 | 0.65 | 0.1 |
| STS-5 | Kapton | 12.7 | 1.50 | 0.99 | 1.5 |
| Witness | Kapton | 25.4 | 2.18 | 0.99 | 2.2 |
| Samples | Kapton | 50.8 | 2.79 | 0.99 | 2.8 |
| | Kapton, Black | 25.4 | 1.35 | 0.99 | 1.4 |
| | Mylar | 12.7 | 2.16 | 0.99 | 2.2 |
| | Mylar | 25.4 | 1.83 | 0.99 | 1.8 |
| | Mylar | 50.8 | 1.50 | 0.99 | 1.5 |
| | Tedlar, Clear | 12.7 | 1.30 | 0.99 | 1.3 |
| | Tedlar, White | 25.4 | <0.50 | 0.99 | <0.5 |
| | Teflon FEP & TFE | 12.7 | <0.50 | 0.99 | <0.5 |
| | Kapton (Coated), DC1-2755 | 12.7 | (Kapton)<0.50 | 0.99 | <0.5 |
| | T-650 | 12.7 | (Kapton)<0.50 | 0.99 | <0.5 |

Continued...

TABLE 1. SUMMARY OF ATOMIC OXYGEN REACTION EFFECTS FOR VARIOUS THIN FILMS USED ON SPACECRAFT
(From Ref. 3)
Continued

| Shuttle Flight | Thin Film Material | Thickness μm (a) | Thickness Loss μm | Fluence $10^{20}$ atoms/cm$^2$ | Reaction Efficiency $10^{-24}$ cm$^3$/atom (b) |
|---|---|---|---|---|---|
| STS-8 | Kapton | 12.7 | 10.4 | 2.98 | 3.5 |
| Witness | Kapton | 25.4 | 9.5 | 2.98 | 3.2 |
| Samples | Kapton | 50.8 | 11.0 | 2.98 | 3.7 |
| | Mylar A | 12.7 | 13.0 | 2.98 | 4.4 |
| | Mylar A | 40.6 | 12.0 | 2.98 | 4.0 |
| | Mylar D | 50.8 | 9.9 | 2.98 | 3.3 |
| | Tedlar, Clear | 12.7 | 11.2 | 2.98 | 3.8 |
| | Polyethylene | 20.3 | 11.5 | 2.98 | 3.9 |
| | Teflon TFE | 12.7 | <0.1 | 2.98 | <0.03 |
| | Kapton F (FEP Coated) | 30.5 | <0.1 | 2.98 | <0.03 |

[a]Note: Film thicknesses of 12.7, 25.4 and 50.8 μm corresponds to 0.5, 1.0 and 2.0 mils, respectively.
[b]Most probable error is +30 to 40%.

TABLE 2. DESCRIPTION OF MATERIALS TESTED IN ATOMIC OXYGEN BEAM FACILITY (3 CM FROM ORIFICE)

| Samples | | Exposure Time (hrs) Vacuum ($10^{-5}$ torr) | Exposure Time (hrs) Atomic* Oxygen | Area ($cm^2$) | Initial Weight (gms) | Final Weight (gms) |
|---|---|---|---|---|---|---|
| Graphite/Epoxy Hercules AS1/3501-6 (0.318 mm thick) | Control | 1152.30 | - | 9.74 | .431902 | .430355 |
| | Target | See * below | 264.47 | 9.74 | .480055 | .477724 |
| Kapton H (0.127 mm thick) | Control | 798.25 | - | 22.44 | .391665 | .390825 |
| | Target | See * below | 187.41 | 17.82 | .326570 | .325876 |

*Targets were subjected to same vacuum duration as control samples, but ~1 $cm^2$ area exposed to atomic oxygen on one face for duration noted: flux $\approx 10^{15}$ atoms/$cm^2$-sec; energy ≈0.14 eV.

TABLE 3. SUMMARY OF MASS LOSS RESULTS*

| Material | Model** | % Mass Loss Vacuum | % Mass Loss Atomic Oxygen | Mass Loss Rate/Unit Area (gms/$cm^2$-sec) Vacuum | Mass Loss Rate/Unit Area (gms/$cm^2$-sec) Atomic Oxygen |
|---|---|---|---|---|---|
| Graphite/Epoxy Hercules AS1/3501-6 | a | .358 | .127 | $3.83\times10^{-11}$ | $6.42\times10^{-10}$ |
| | b | .354 | .132 | $3.83\times10^{-11}$ | $6.64\times10^{-10}$ |
| Kapton H | a | .214 | - | $1.30\times10^{-11}$ | - |
| | b | .213 | - | $1.30\times10^{-11}$ | - |

*The data presented are based on an estimated flux of ~$10^{15}$ atoms/$cm^2$-sec and energy level ≈0.14 eV. The fluence ≈$10^{21}$ and $7\times10^{20}$ atoms/$cm^2$ for graphite/epoxy and Kapton, respectively.
**See secion 4.3 for model descriptions.

TABLE 4. CONTACT ANGLE AND SURFACE TENSION VALUES

| Samples | | Angle (degrees) | Tension ($mJ/m^2$) |
|---|---|---|---|
| Graphite/Epoxy Hercules ASI/3501 | Exposed | 40.00 | 3.167 |
| | | 41.25 | 3.497 |
| | | 40.00 | 3.167 |
| | | 42.50 | 3.847 |
| | | 40.67 | 3.340 |
| | Avg. | 40.88 | 3.404 |
| | Unexposed | 48.33 | 5.744 |
| | | 46.33 | 5.045 |
| | | 48.00 | 5.624 |
| | | 47.67 | 5.505 |
| | Avg. | 47.58 | 5.480 |
| Kapton | Exposed | 52.00 | 7.159 |
| | | 51.00 | 6.756 |
| | | 54.00 | 8.002 |
| | | 52.33 | 7.434 |
| | Avg. | 52.33 | 7.338 |
| | Unexposed | 44.33 | 4.396 |
| | | 46.00 | 4.933 |
| | | 45.56 | 4.823 |
| | | 44.33 | 4.396 |
| | Avg. | 45.08 | 4.637 |

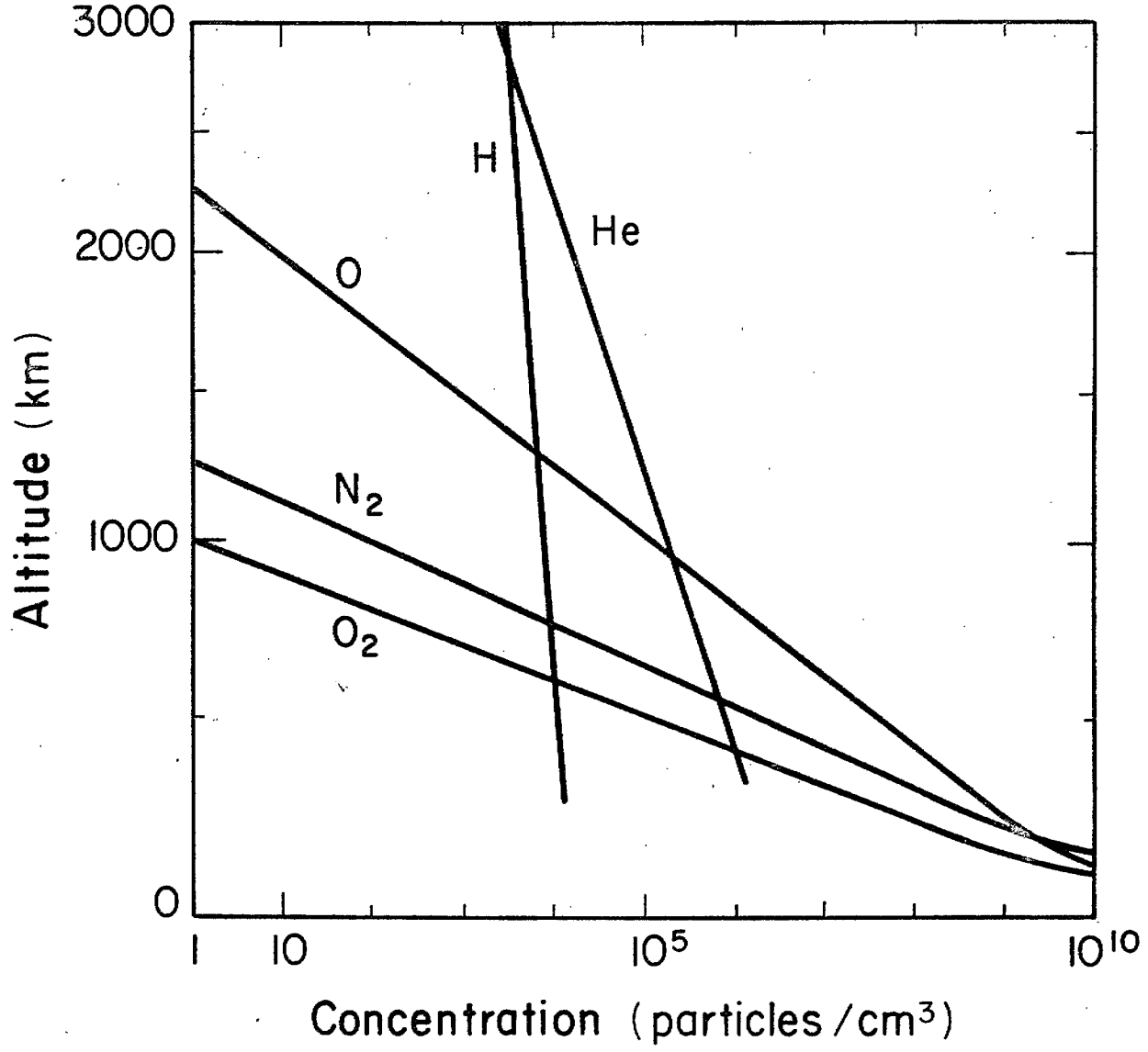


Fig. 1 CONCENTRATION OF ATMOSPHERIC CONSTITUENTS

(Ref. 5)

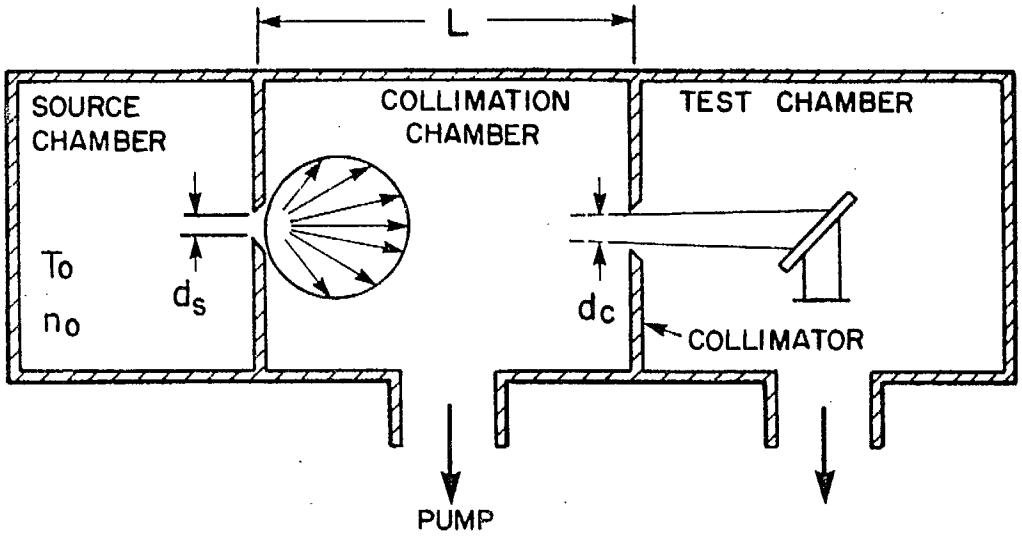


CLASSICAL MOLECULAR BEAM

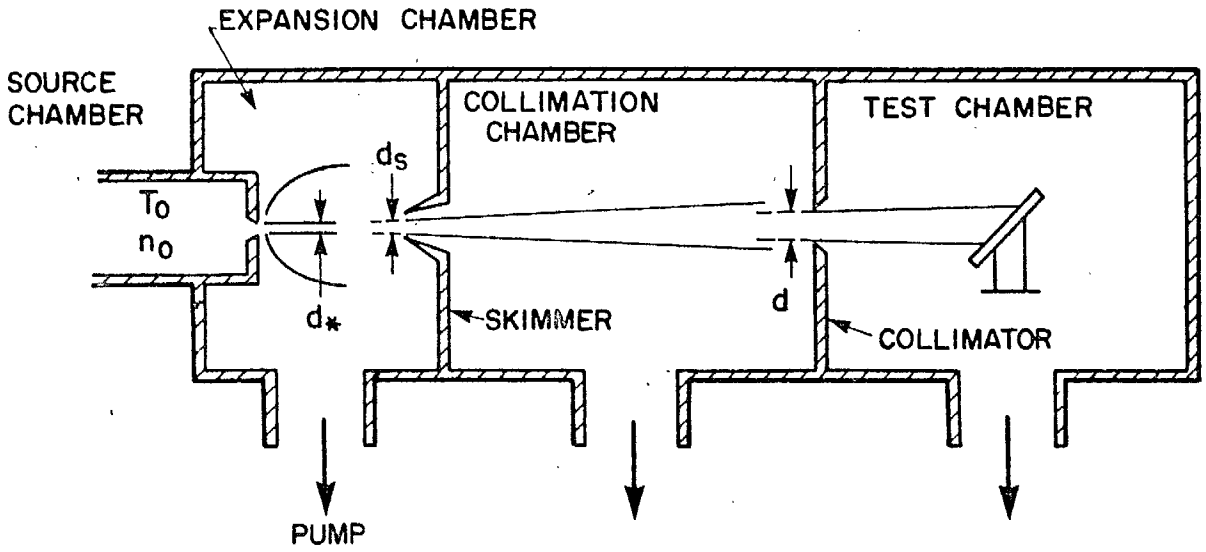


NOZZLE SOURCE BEAM

Fig. 2 TWO SYSTEMS FOR MOLECULAR BEAM GENERATION

( Ref. 4 )

Diffusion
Pump
Valve

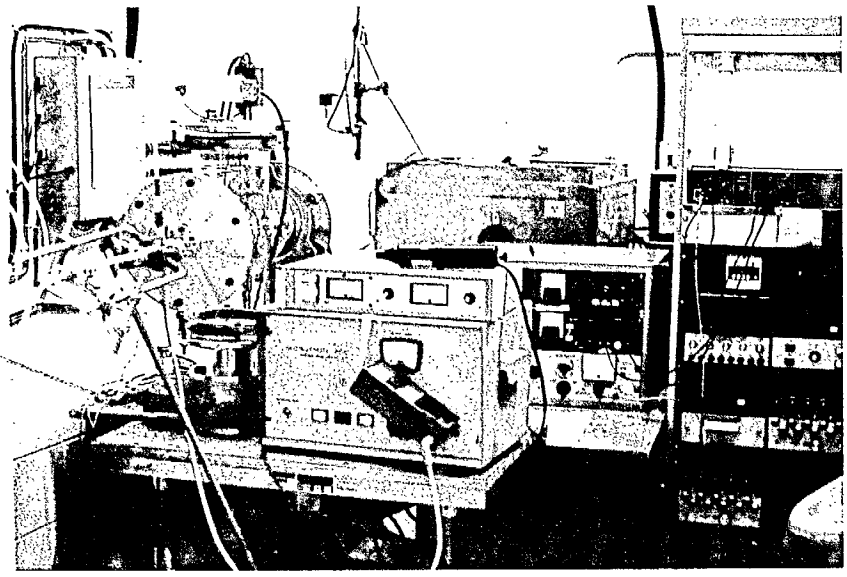

FIG. 3

A. Microwave Generator

B. Ionization Vacuum Gauge

C. Tesla Coil

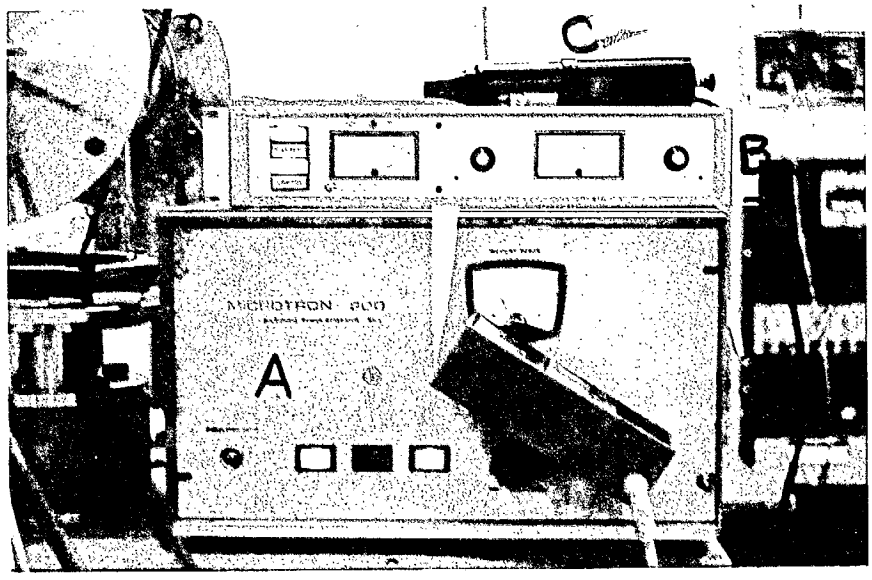


FIG. 4

A. Cooling Air Tube

B. Tuning Cavity

C. Roughing Pump Valve

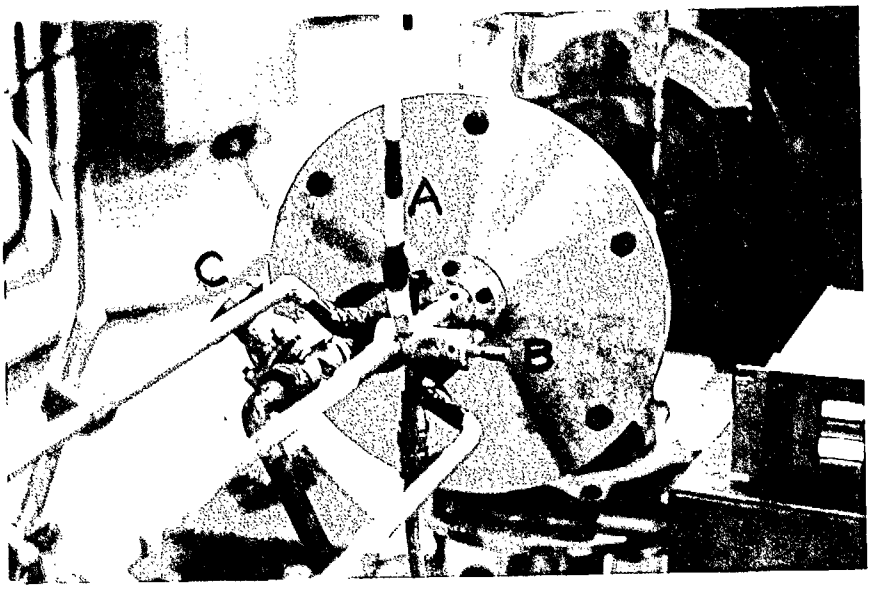


FIG. 5

D. Ionization Coil Pick-up

E. Vacuum Vessel

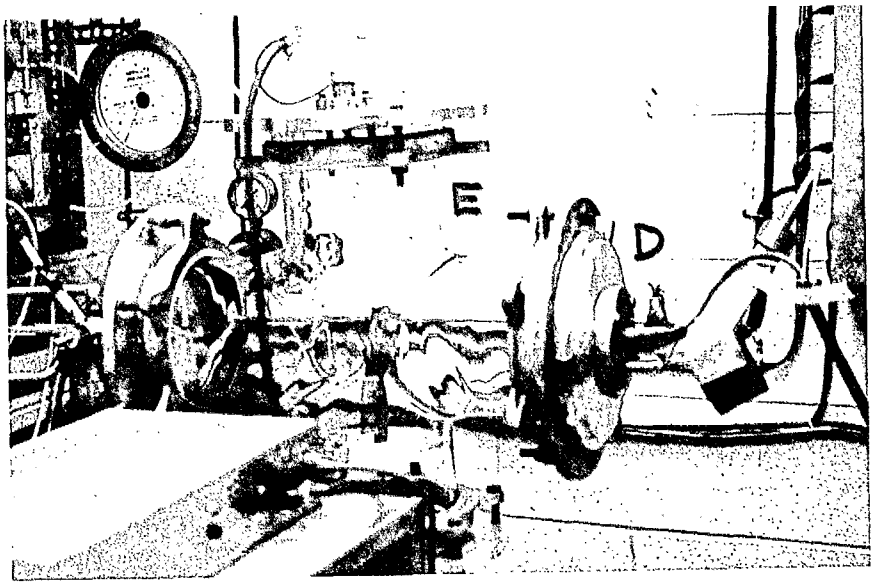


FIG. 6

Mass
Spectrometer
Unit

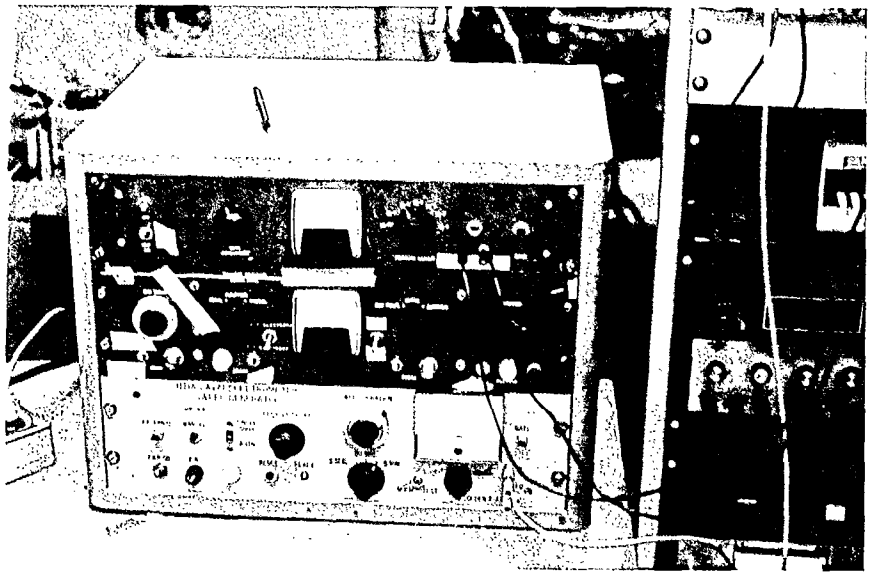

FIG. 7

A. Cooling Air Valve

B. Needle Valve

C. Venting Valve

D. Manometer Valve

E. Feed Valve

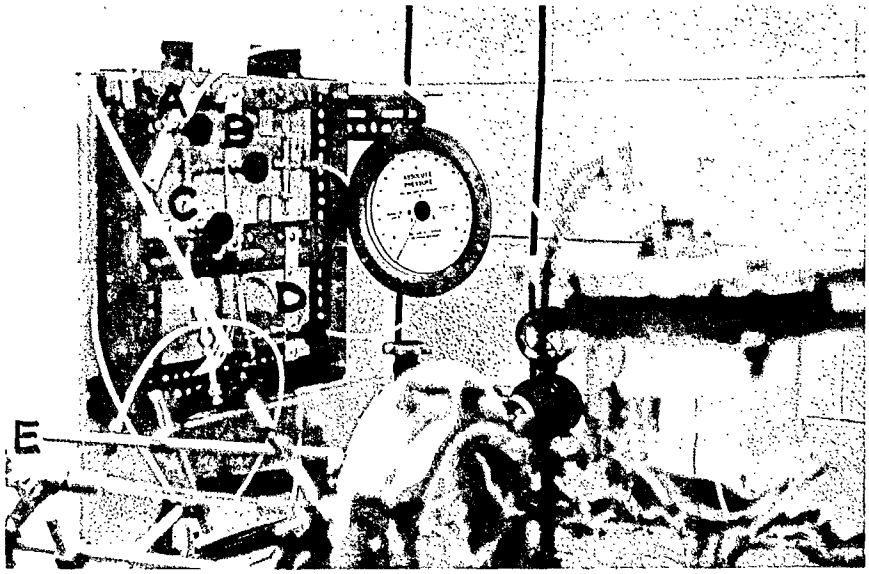


FIG. 8

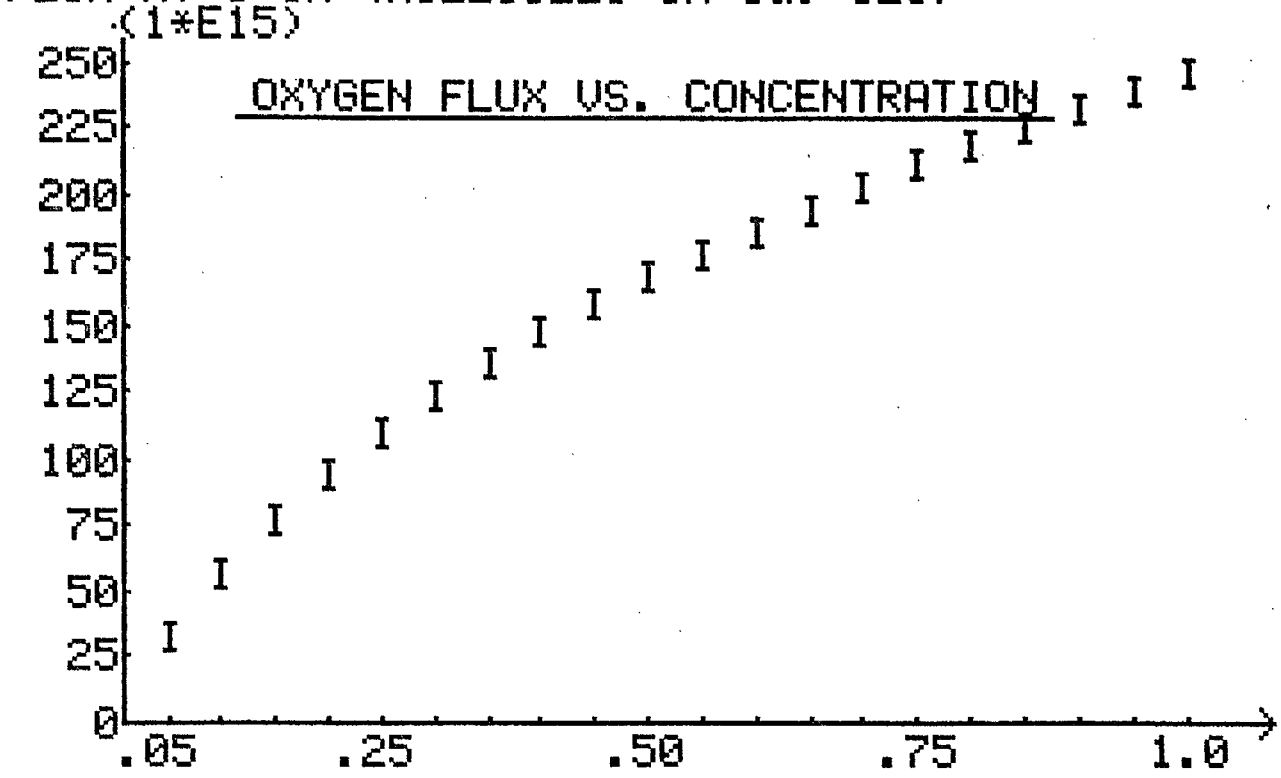


FIG. 9 FRACTION OF O2 IN MIXTURE

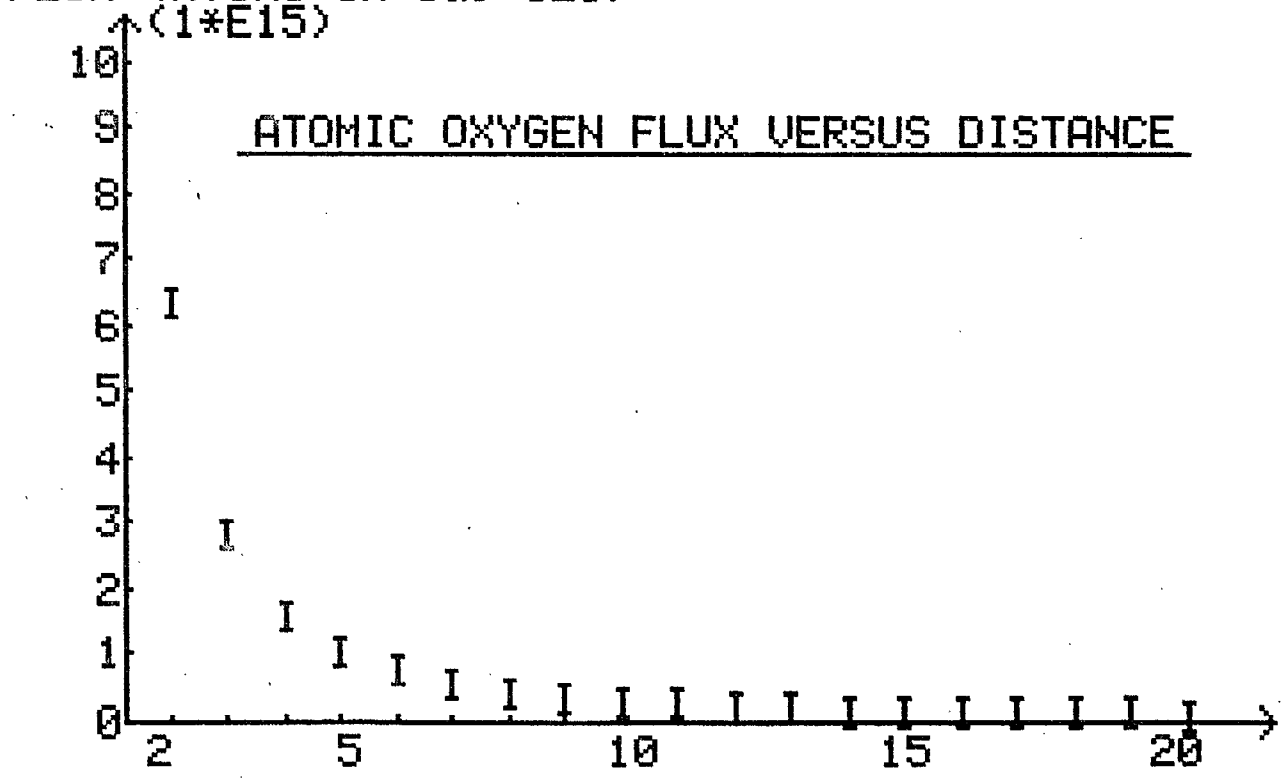


FIG. 10 DISTANCE FROM ORIFICE (CM)

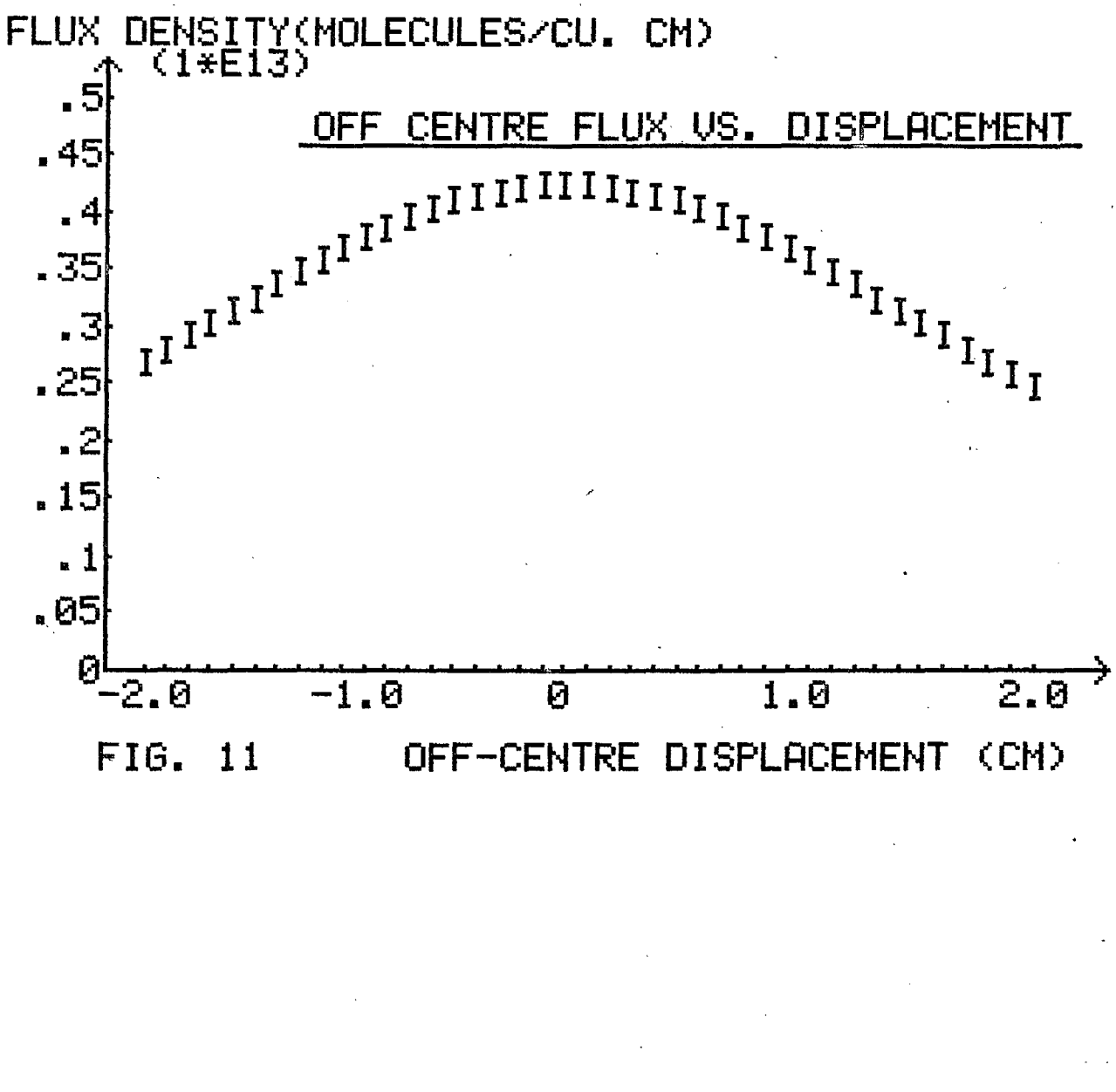
FLUX DENSITY(MOLECULES/CU. CM)
(1*E13)
OFF CENTRE FLUX VS. DISPLACEMENT
.5
.45
.4
.35
.3
.25
.2
.15
.1
.05
0
-2.0
-1.0
0
1.0
2.0
OFF-CENTRE DISPLACEMENT (CM)

FIG. 11

Mass Spectrograph of Residuals in Vacuum Vessel

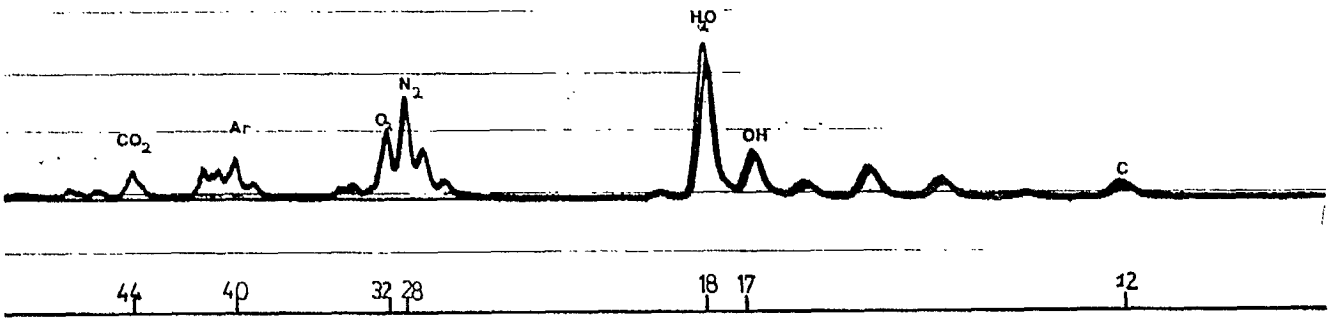


Fig. 12

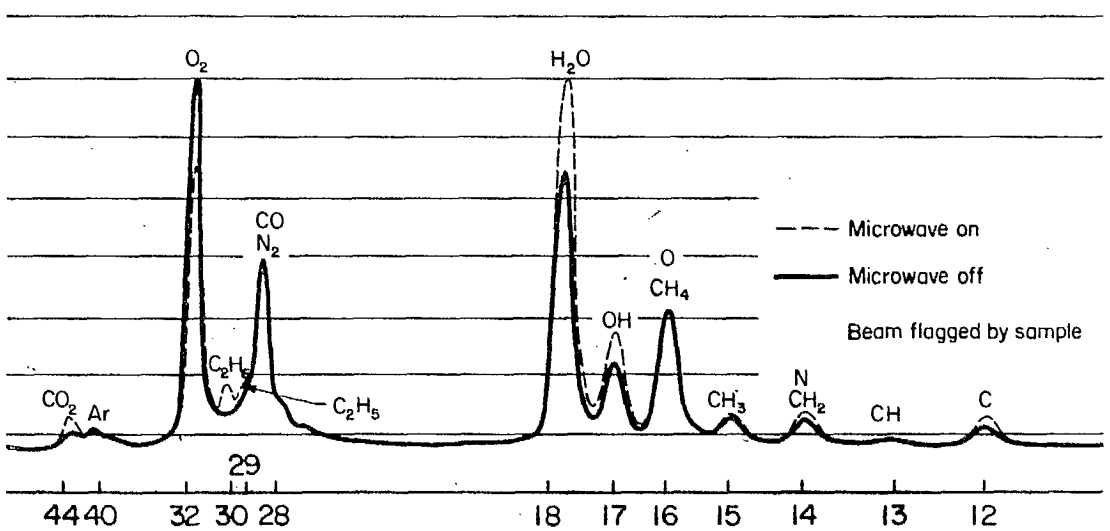


FIG. 13 GRAPHITE/EPOXY: MASS SPECTROGRAPH

GRAPHITE / EPOXY:

Mass Spectrograph

Microwave generator and carrier gas on
Beam flagged with sample

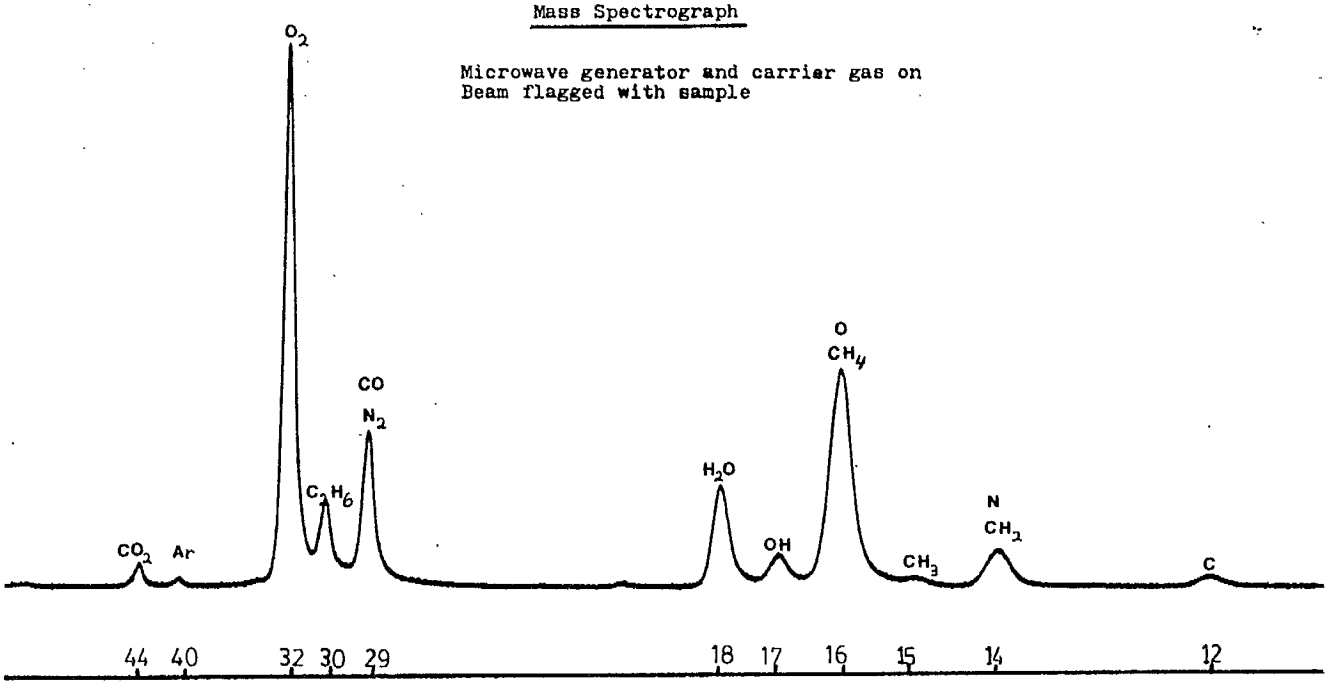


Fig. 14

GRAPHITE / EPOXY:

Mass Spectrograph

Microwave generator off
Carrier gas on
Beam flagged by sample

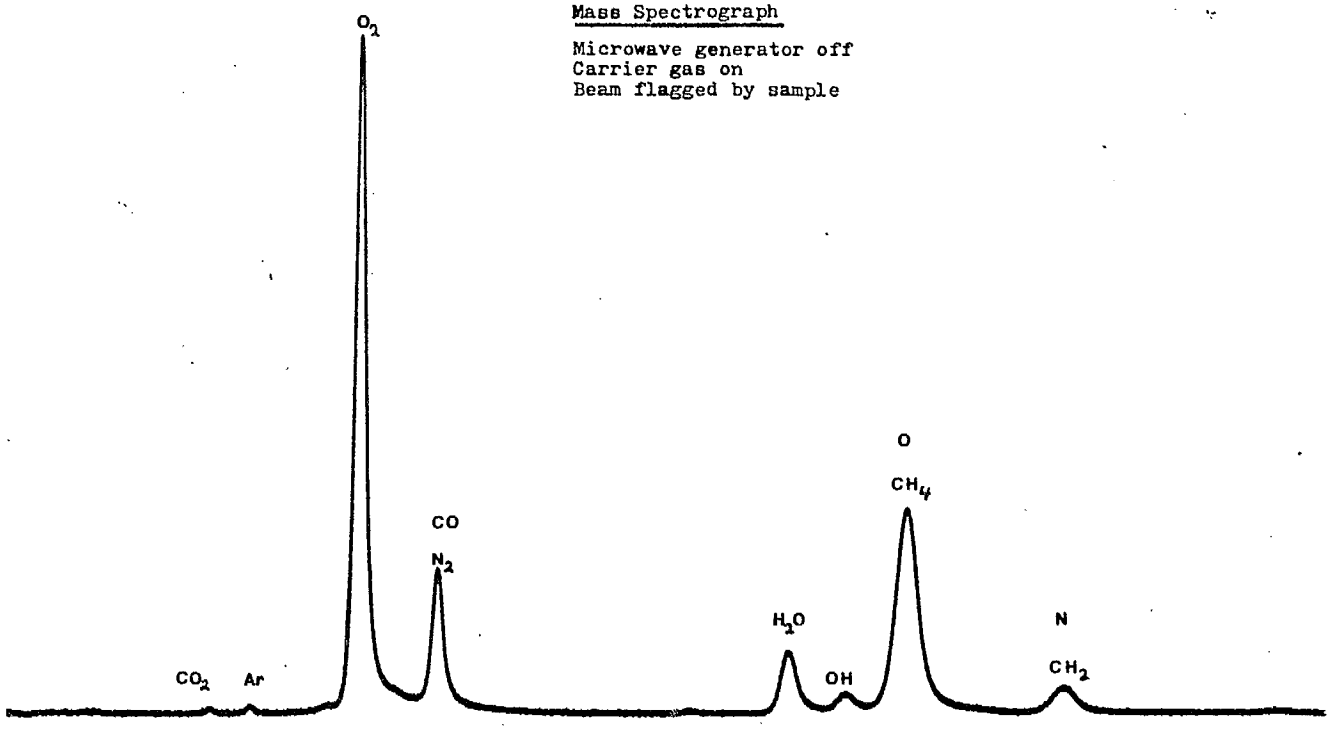


Fig. 15

KAPTON : Mass Spectrograph

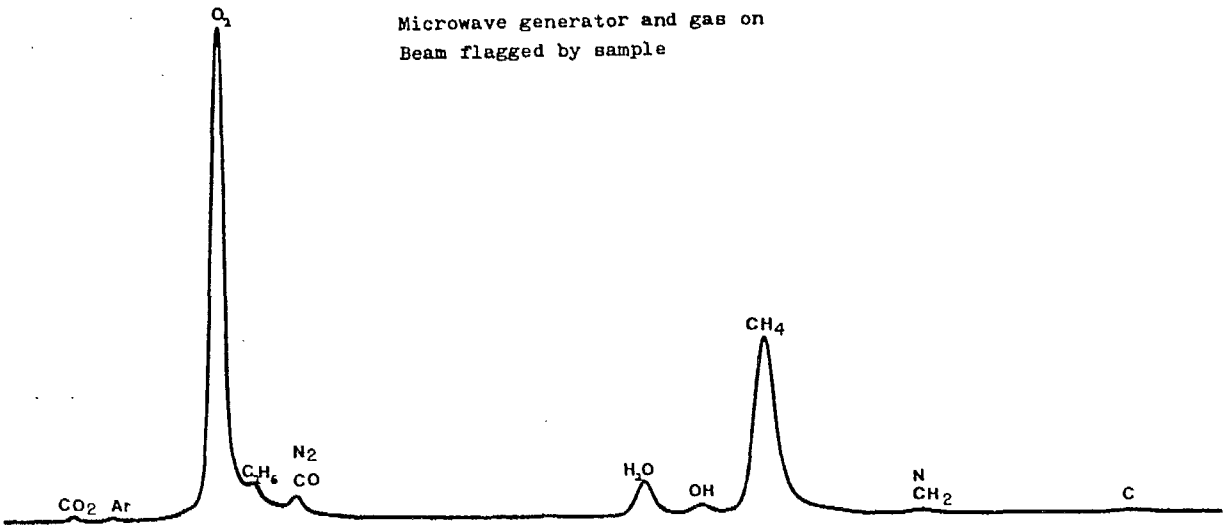


Fig. 16

KAPTON: Mass Spectrograph

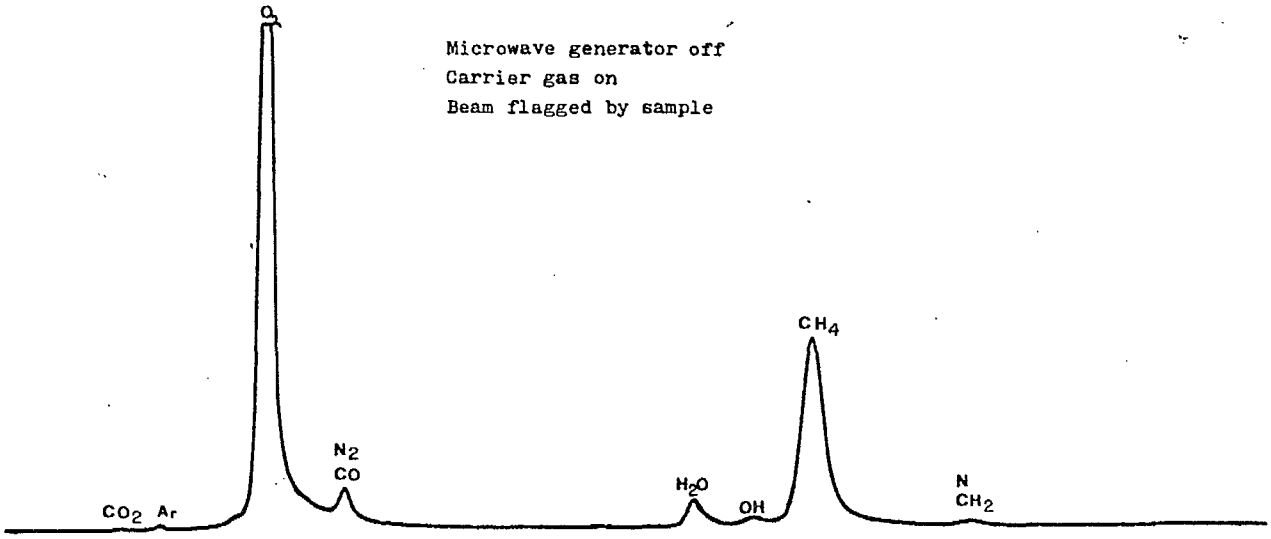


Fig. 17

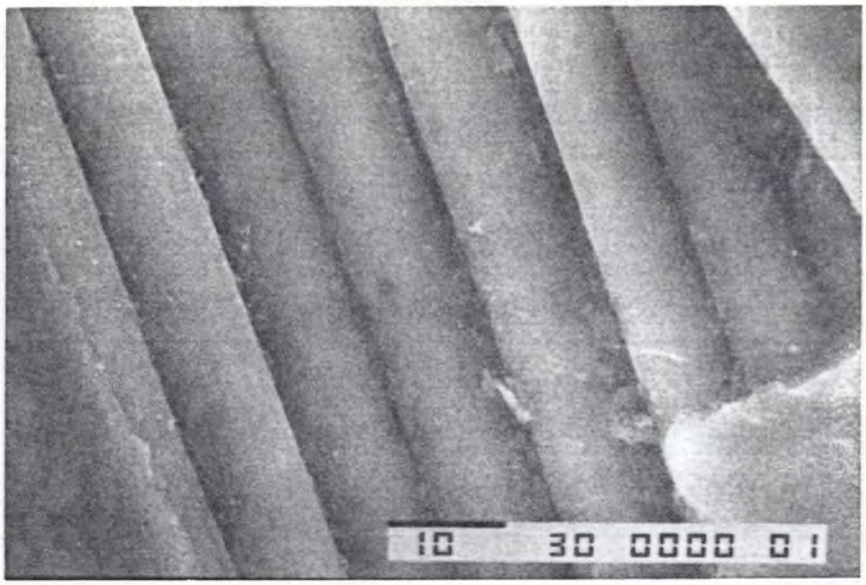


FIG. 18 SEM PHOTOGRAPH OF UNPREPARED, UNEXPOSED GRAPHITE/EPOXY SAMPLE (1500 X)

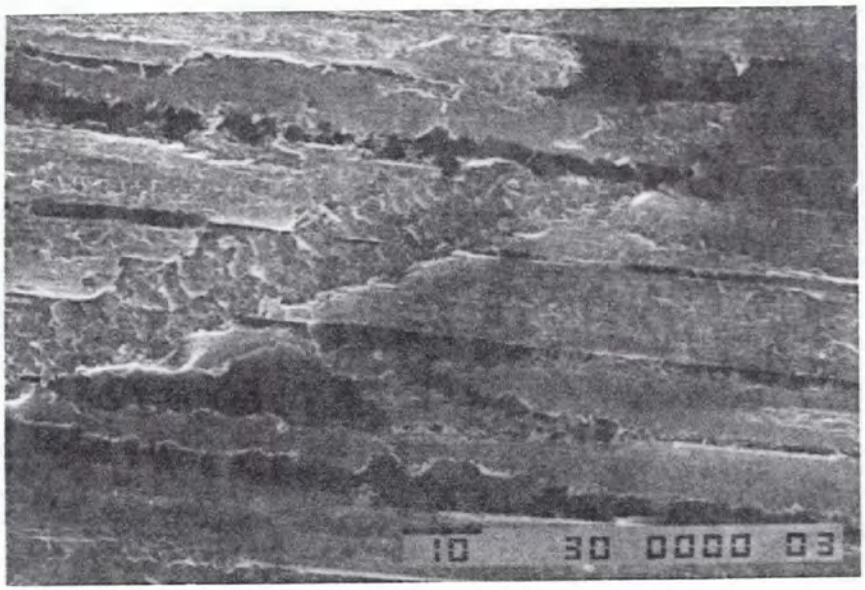


FIG. 19 SEM PHOTOGRAPH OF PREPARED, UNEXPOSED GRAPHITE/EPOXY SAMPLE (1000 X)

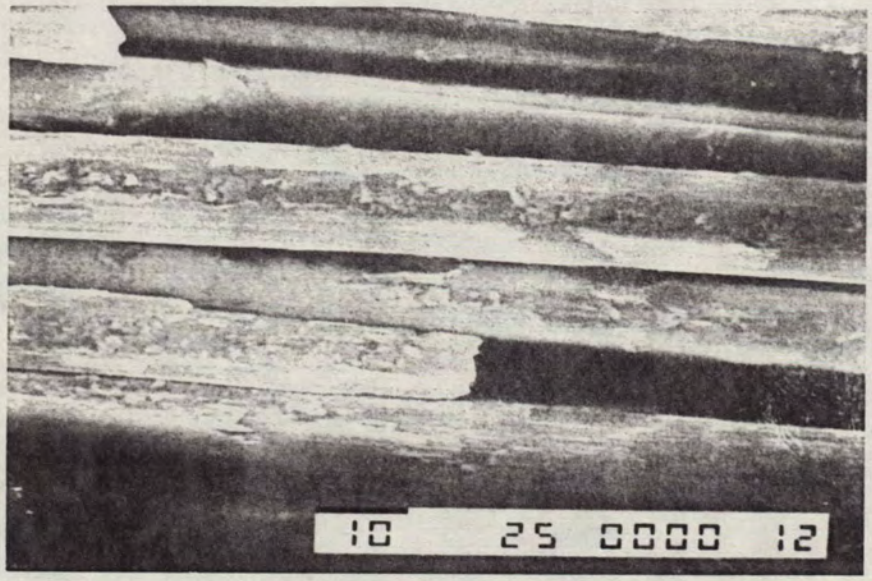


FIG. 20 SEM PHOTOGRAPH OF PREPARED, EXPOSED GRAPHITE/EPOXY SAMPLE (1000 X)

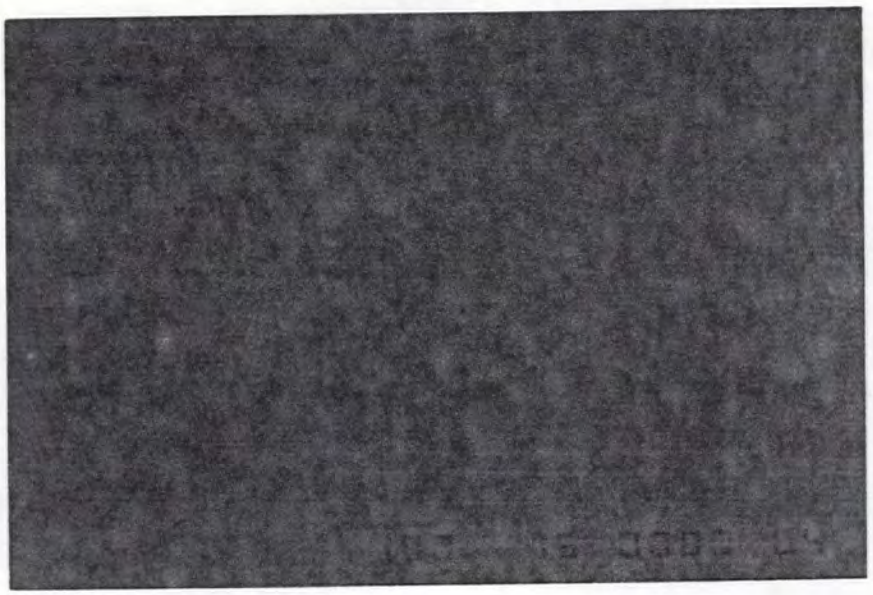

FIG. 21 SEM (NORMAL) PHOTOGRAPH OF UNEXPOSED KAPTON CONTROL SAMPLE (100 X)

FIG. 22 SEM Y-MODULATION PHOTOGRAPH OF UNEXPOSED KAPTON CONTROL SAMPLE (100 X)

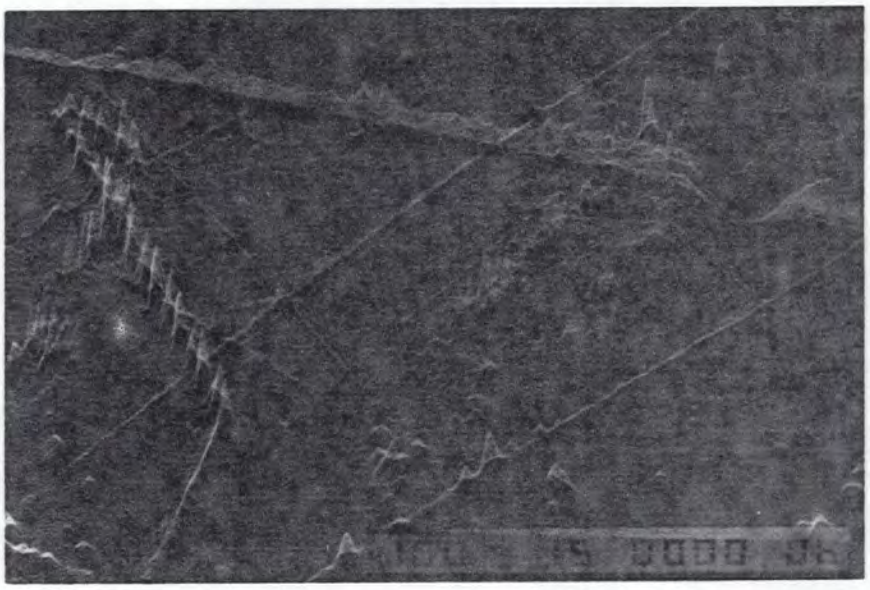

FIG. 23 SEM Y-MODULATION PHOTOGRAPH OF UNEXPOSED KAPTON CONTROL SAMPLE (100 X)

FIG. 24 SEM Y-MODULATION PHOTOGRAPH OF UNEXPOSED KAPTON CONTROL SAMPLE (100 X)

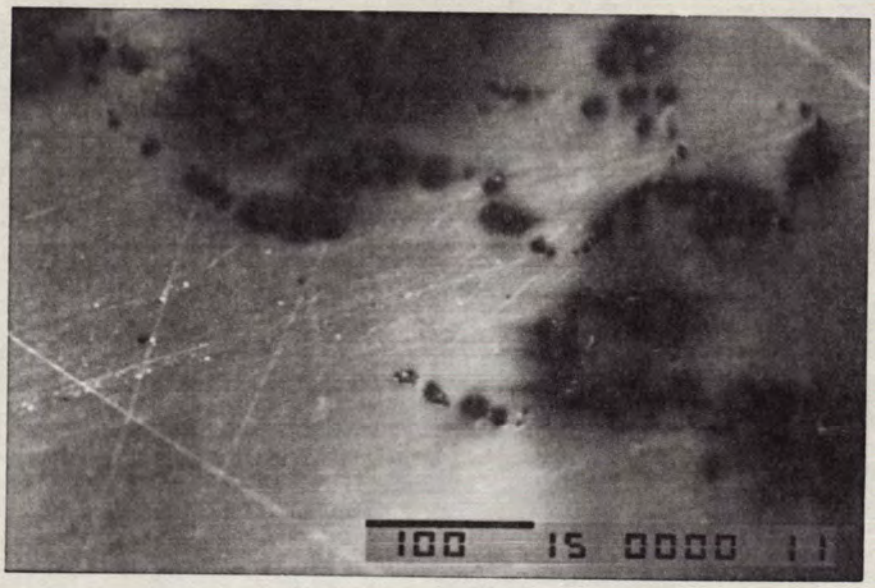


FIG. 25 SEM (NORMAL) PHOTOGRAPH OF EXPOSED KAPTON SAMPLE

(200 X)

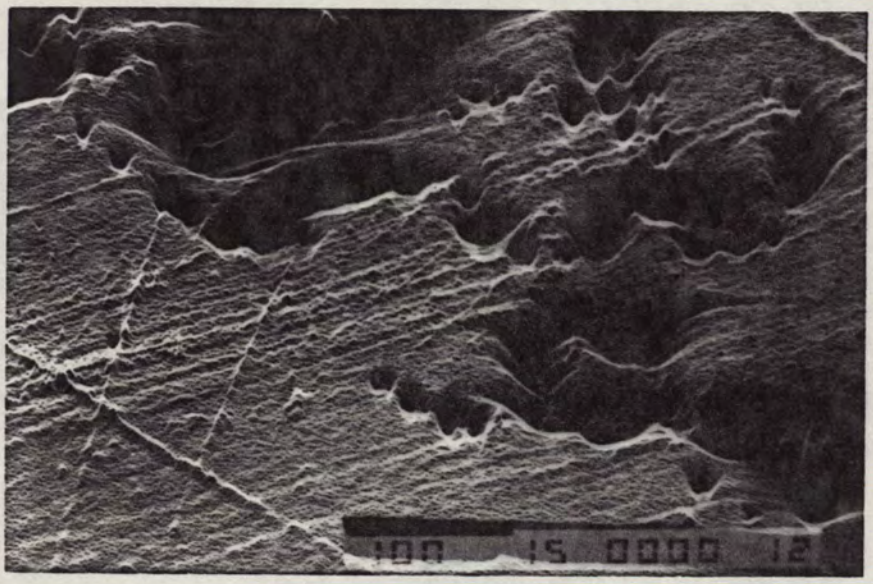


FIG. 26 SEM Y-MODULATION PHOTOGRAPH OF EXPOSED KAPTON SAMPLE

(200 X)


FIG. 27 SEM (NORMAL) PHOTOGRAPH OF EXPOSED KAPTON SAMPLE
(1500 X)

FIG. 28 SEM Y-MODULATION PHOTOGRAPH OF EXPOSED KAPTON SAMPLE
(1500 X)